

# Sodium Incorporation for Performance Improvement of Solution-Processed Submicron $\text{CuIn}(\text{S},\text{Se})_2$ Thin Film Solar Cells

Yao Gao, Guanchao Yin,\* and Martina Schmid\*

Low-cost solution-processed  $\text{CuIn}(\text{S},\text{Se})_2$  (CISSe) has great potential for large-scale production of photovoltaics (PV). However, low power conversion efficiency caused by poor crystallinity is one of the main drawbacks compared to vacuum-processed CISSe solar cells. In this work, three strategies for sodium (Na) incorporation into solution-processed CISSe by soaking in sodium chloride (NaCl) aqueous-ethanol solution [1 molarity (M) for 10 minutes (min)], either prior to absorber deposition (pre-deposition treatment, Pre-DT), before selenization (pre-selenization treatment, Pre-ST), or after selenization (post-selenization treatment, PST) are researched. The Pre-ST CISSe solar cells achieve a better PV performance than those from the other two strategies of Na incorporation. For optimization, soaking times (5, 10, and 15 min) and NaCl concentrations (from 0.2 to 1.2 M) of the Pre-ST are researched. The highest efficiency achieved is 9.6% with an open-circuit voltage ( $V_{oc}$ ) of 464.5 mV, a short-circuit current density ( $j_{sc}$ ) of  $33.4 \text{ mA cm}^{-2}$ , and a fill factor (FF) of 62.0%. Compared to the reference CISSe solar cell,  $V_{oc}$ ,  $j_{sc}$ , FF, and efficiency of the champion Pre-ST CISSe device are improved absolutely by 61.0 mV,  $6.5 \text{ mA cm}^{-2}$ , 9%, and 3.8%, respectively. Simultaneously, the open-circuit voltage deficit, the back contact barrier, and the bulk recombination are found to be reduced for Pre-ST CISSe.

solar energy materials due to the high power conversion efficiency (the champion efficiency of the  $2.5 \mu\text{m}$  thick absorber devices achieved 23.35%).<sup>[1]</sup> The high-performance CIGSs solar cells are deposited by vacuum processes, including co-evaporation and sputtering.<sup>[1,2]</sup> Fabrication of CIGSe via a vacuum-based process can achieve a high-quality absorber and good compositional control. However, vacuum-based processes rely on highly pure metal sources, high energy input, and high vacuum conditions, resulting in high operational costs.<sup>[3]</sup> A non-vacuum and low-cost solution process has been explored for CIGSe thin film solar cell fabrication because it can reduce energy consumption and costs. So far, the highest efficiency of solution-processed CIGSe achieves 18.1% (certified 17.3%) via a hydrazine-based solution.<sup>[4]</sup> However, hydrazine is undesirable for mass production owing to its high toxicity and the absorber fabrication process required to be carried out in a glovebox. Many alternative solvents have been utilized for CIGSe absorber fabrication. Amine-thiol (SH-based) solvents have been applied

## 1. Introduction


Copper indium gallium disulfoselenide [ $\text{Cu}(\text{In}_x\text{Ga}_{1-x})(\text{S},\text{Se})_2$ ] is considered one of the most promising

for CIGSs solar cell research achieving 16.4% efficiency by designing a copper-poor ordered vacancy compound (OVC) layer.<sup>[5]</sup> However, thiol and amine group solvents are still highly toxic, and the toxic  $\text{H}_2\text{S}$  gas will form during the annealing process of precursor film fabrication. Several non-toxic solvents have thus been tried for chalcopyrite thin film fabrication. The champion efficiency of a CIGSs solar cell fabricated from non-toxic alcohol-based solution has reached 14.4%.<sup>[6]</sup> Yet, a residual carbon layer is observed at the rear interface of alcohol-based CIGSs, and the open circuit voltage deficit ( $V_{oc,def}$ ) is large. Fabrication of CIGSe solar cells from dimethyl sulfoxide (DMSO) molecular precursor solution has achieved 17.7% efficiency.<sup>[7]</sup> However, the solubility of  $\text{In}(\text{DMSO})\text{Cl}_3$  is only 0.1 molarity (M) at room temperature and 0.5 M at  $120^\circ\text{C}$ .<sup>[8]</sup> Therefore, the precursor ink should remain at a high temperature during spin-coating. In contrast to the DMSO solution, dimethylformamide thiourea (DMF-TU) solution can dissolve  $\text{InCl}_3$  to form a stable molecular ink (0.65 M at room temperature and up to 1.8 M at  $120^\circ\text{C}$ ).<sup>[8,9]</sup> In addition, the DMF-TU solution can also dissolve  $\text{Cu}(\text{II})$ ,  $\text{Zn}(\text{II})$ ,  $\text{Ge}(\text{IV})$ ,  $\text{Ag}(\text{I})$ , and  $\text{Cu}(\text{I})$  very well, which can be utilized for kesterite and chalcopyrite absorber fabrication.<sup>[9]</sup> A

Y. Gao, M. Schmid  
Faculty of Physics and Center for Nanointegration Duisburg-Essen  
(CENIDE)

University of Duisburg-Essen  
Forsthausweg 2, 47057 Duisburg, Germany  
E-mail: martina.schmid@uni-due.de

G. Yin  
School of Materials Science and Engineering  
Wuhan University of Technology  
Luoshi Road 122, Wuhan 430070, China  
E-mail: guanchao.yin@whut.edu.cn

 The ORCID identification number(s) for the author(s) of this article can be found under <https://doi.org/10.1002/small.202302581>

© 2023 The Authors. Small published by Wiley-VCH GmbH. This is an open access article under the terms of the Creative Commons Attribution License, which permits use, distribution and reproduction in any medium, provided the original work is properly cited.

DOI: 10.1002/small.202302581

dimethylformamide (DMF) molecular solution has been applied for CIGSSe absorber fabrication, resulting in densely packed large grains without a fine-grained layer,<sup>[10]</sup> and the corresponding solar cells presented 15.2% maximum efficiency (1.2  $\mu\text{m}$  thick absorber).<sup>[10a]</sup>

Another attempt for low-cost processes is reducing the absorber thickness, which can decrease the consumption of scarce indium.<sup>[11]</sup> However, when the absorber layer thickness drops below 1  $\mu\text{m}$  (submicron), the efficiency of the device degrades severely and the risk of shunts increases remarkably.<sup>[12]</sup> Passivation of shunt paths will improve the photovoltaic (PV) performance of submicron CIGSSe solar cells which can, e.g., be achieved by alkali element post-deposition treatment.<sup>[2c,13]</sup> Alkali incorporation can reduce the defect density and improve the absorber quality, which will enhance the open circuit voltage ( $V_{oc}$ ) and fill factor ( $FF$ ), resulting in efficiency improvement.<sup>[2c,13]</sup> Furthermore, carrier recombination and open circuit voltage deficit ( $V_{oc,def}$ ) can be reduced by the incorporation of alkali elements into CIGSSe absorbers.<sup>[14]</sup> However, excessive alkali incorporation will deteriorate the absorber morphology (formation of pinholes and decrease in grain size), leading to inferior PV performance.<sup>[15]</sup> Therefore, it is crucial to control the alkali content for obtaining highly efficient CIGSSe solar cells.

Alkali post-deposition treatment (PDT) has been extensively studied for CIGSe absorbers fabricated by co-evaporation, remarkably improving PV performance. Sodium was widely applied for alkali incorporation, affecting the grain size, crystal orientation, p-type conductivity,  $V_{oc}$ , and  $FF$ .<sup>[16]</sup> The most common path for sodium incorporation in the co-evaporation process is the PDT, i.e., depositing a thin layer of sodium fluoride (NaF) after CIGSSe absorber growth. NaF PDT can passivate the grain boundaries and form a Cu-poor surface, leading to PV performance improvement.<sup>[13b,17]</sup> Compared to absorber fabrication by co-evaporation, Na atoms can be introduced at different steps of CIGSSe growth from precursor solution. For example, Na ions can be added into the precursor solution, prior to the precursor deposition, before or after selenization. Compared to NaF, sodium chloride (NaCl) offers low cost, benign nature, and good solubility in water.<sup>[15]</sup> The typical strategy for sodium incorporation into solution-processed CIGSSe solar cells is therefore soaking the precursor thin film in NaCl solution.<sup>[18]</sup> However, there is rare comparative research on Na incorporation using different strategies for solution-processed CIGSe. Therefore, corresponding research will be of great interest.

In this work, we focus on submicron (here 820 nm absorber layer thickness) solution-processed  $\text{CuIn}(\text{S},\text{Se})_2$  (CISSe) solar cells and aim at performance enhancement by Na incorporation. Sodium chloride aqueous-ethanol with 1 mol  $\text{L}^{-1}$  (1 M NaCl) is applied for sodium incorporation by utilizing pre-deposition treatment (Pre-DT), pre-selenization treatment (Pre-ST), and post-selenization treatment (PST). The PV characteristics of the Pre-ST CISSe solar cells are better than those of the reference CISSe solar cells (without sodium treatment) and those processed by Pre-DT or PST. The soaking times (5, 10, and 15 min) and the NaCl concentration (0.2–1.2 M with a step of 0.2 M) of the Pre-ST are also researched. When the precursor films are soaked in 1 M NaCl for 10 min, CISSe solar cells achieve an efficiency of 9.6%. Compared to the reference CISSe, the open-circuit voltage, short-circuit current density, fill factor, and efficiency of the

champion Pre-CISSe device are improved absolutely by 61.0 mV, 6.5 mA  $\text{cm}^{-2}$ , 9%, and 3.8%, respectively. Simultaneously, the open circuit voltage deficit and the back barrier height are remarkably reduced after NaCl treatment.

## 2. Results

### 2.1. Effect of Na Incorporation Strategies

To research the effect of Na incorporation strategies, 1 M NaCl aqueous-ethanol solution (volume ratio of ultra-pure water to ethanol is 1:1) was utilized for Na incorporation. NaCl was introduced in various experiment stages (Figure 1): either prior to absorber deposition (pre-deposition treatment, Pre-DT), before selenization (pre-selenization treatment, Pre-ST), or after selenization (post-selenization treatment, PST).

Raman spectroscopy measurements are utilized to identify the purity of the CISSe thin films (Figure 2). All absorbers show a strong peak at short wavenumbers related to the  $A_1$  vibration mode.<sup>[5,10b,19]</sup> The  $\text{CuInSe}_2$  and  $\text{CuInS}_2$   $A_1$  peaks locate at 172 and 290  $\text{cm}^{-1}$ , respectively.<sup>[20]</sup> For our samples, we find a peak at 184  $\text{cm}^{-1}$  for the reference, and at 179  $\text{cm}^{-1}$  for the Na-treated absorbers. The right-shift of the Raman peak compared to the  $A_1$  mode of pure  $\text{CuInSe}_2$  is attributed to the incorporation of S in the absorber layer.<sup>[19,21]</sup> The more pronounced right-shift of the Raman peak of the reference sample points to a higher S

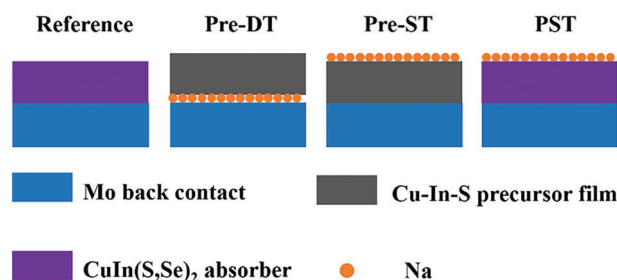


Figure 1. Schematic diagram of sodium treatment strategies.

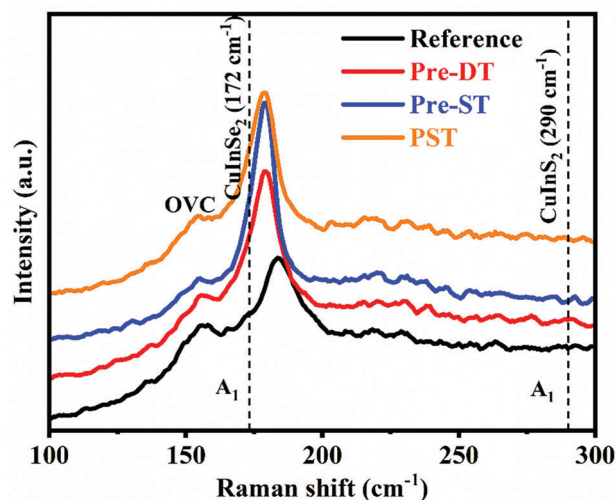
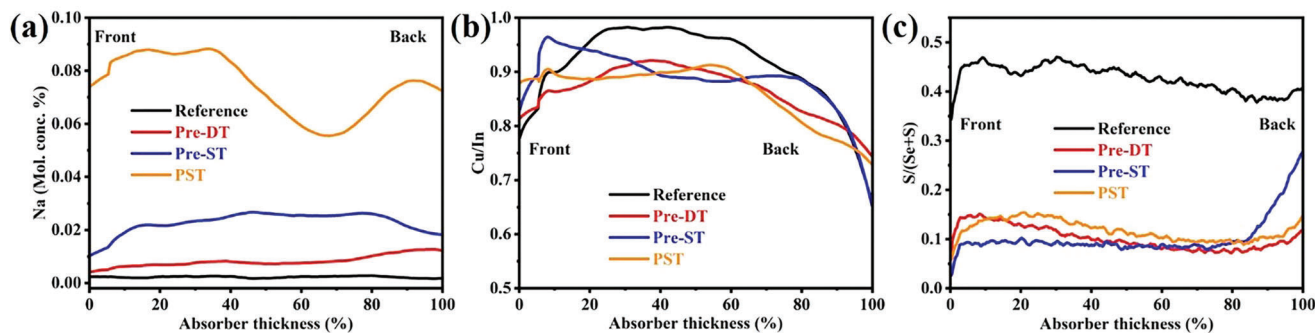


Figure 2. Raman spectra of CISSe absorbers without/with NaCl treatment.



**Figure 3.** a) Na concentration profiles, b) Cu/In, and c) S/(Se+S) ratios of CISSe absorbers without/with Na treatment as measured by GDOES.

concentration compared to CISSe with Na incorporation (compare also the GDOES results shown in **Figure 3c**). Previous literature has proven that the sharp Raman peaks with a small full width at half maximum (FWHM) reflect better CISSe absorber quality.<sup>[19]</sup> The FWHM of the  $A_1$  peak becomes smaller after Na incorporation ( $14.8\text{ cm}^{-1}$  for the reference,  $11.5\text{ cm}^{-1}$  for Pre-DT,  $9.9\text{ cm}^{-1}$  for Pre-ST, and  $10.8\text{ cm}^{-1}$  for PST), indicating that Na incorporation is beneficial to improve the absorber quality. All these CISSe absorbers show a shoulder peak ( $\approx 155\text{ cm}^{-1}$ ) belonging to the  $\text{CuIn}_3(\text{S,Se})_5$  OVC (ordered vacancy compound) layer.<sup>[5,10b]</sup> No impurity characteristic peaks are observed in the CISSe absorbers.

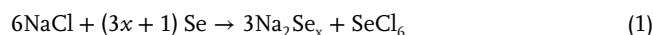
We carry out GDOES measurements on absorbers after electrical characterization and removal of the CdS/i-ZnO/AZO top layers. The resulting concentration of Na, as well as the Cu/In and S/(Se+S) ratios of CISSe without/with Na incorporation, are shown in **Figure 3**. As expected, the Na-doped CISSe absorbers display higher Na concentrations than the reference ( $\text{Na}_{\text{PST}} \gg \text{Na}_{\text{Pre-ST}} > \text{Na}_{\text{Pre-DT}} > \text{Na}_{\text{reference}}$ , see **Figure 3a**). It is reported that Na can occupy the grain boundaries and the grain interior.<sup>[10a,13b]</sup> The post-selenization Na treatment does not further modify the microstructure of the as-selenized CISSe absorber, resulting in a large number of grain boundaries remaining in the absorber.<sup>[13a,15]</sup> Therefore, Na can occupy these grain boundaries in PST CISSe, leading to a significantly higher Na concentration as seen from the GDOES result. The Pre-DT and Pre-ST absorbers display a lower Na concentration at the front surface than in the bulk. A high Na concentration near the front surface of the absorber would hinder the  $\text{Cd}_{\text{Cu}}$  donor defect formation during the CdS CBD process, leading to a lower quality of the pn-junction.<sup>[22]</sup>

CISSe absorbers without/with Na treatment exhibit a Cu-poor composition ( $\text{Cu/In} < 1$ , see **Figure 3b**). The Cu/In ratios firstly increase, then decrease toward the front surface, i.e., the Cu concentration is higher in the bulk (**Figure S1**, Supporting Information). The smaller Cu/In ratios at the front surface of CISSe can be explained by the formation of the  $\text{CuIn}_3(\text{S,Se})_5$  OVC layer, as also the Raman measurements revealed (**Figure 2**).<sup>[16c,23]</sup> The strongest Raman peak related to the OVC is found for the reference sample.

After Na incorporation, the CISSe absorbers exhibit similar S/(S+Se) ratios, which are lower than for the reference CISSe absorber (**Figure 3c**). A higher Se concentration can be correlated to Na assisting the Se diffusion into the absorber via the formation

of a  $\text{Na}_2\text{Se}_x$  liquid phase (see also **Figure S1**, Supporting Information for the individual element distributions).<sup>[10a,13c]</sup> Thus, Na is beneficial to promote the substitution of S by Se during the high-temperature selenization.

Cross-sectional SEM images of CISSe absorbers without/with Na incorporation are shown in **Figure 4**. The absorber thickness of these CISSe devices is  $\approx 820\text{ nm}$ . The reference CISSe, the Pre-ST, and the PST CISSe absorber present a double-layer structure with a fine-grained layer on the bottom and a large-grained layer on top. The Pre-DT CISSe absorber exhibits a triple-layer structure: a dense layer of fine grains on the bottom, a thick layer consisting of large grains on top, and an assembly of loosely connected grains in between.<sup>[24]</sup> These loose grains may be attributed to the residual chlorine ion ( $\text{Cl}^-$ ).<sup>[15]</sup> Similarly to the formation of  $\text{SeF}_6$  when using NaF for Na incorporation, the chlorine ion ( $\text{Cl}^-$ ) can be removed by forming  $\text{SeCl}_6$  due to the reaction between  $\text{Cl}^-$  and Se vapor.<sup>[15,25]</sup> The possible chemical equation between NaCl and Se vapor is shown below:



Large CISSe grains are firstly formed on top of the absorber during the high-temperature selenization.<sup>[10b,24]</sup> This CISSe top layer will hinder the volatilization of  $\text{SeCl}_6$  coming from the rear in the case of Pre-DT, leading to residual  $\text{Cl}^-$  inside the CISSe absorber.<sup>[15]</sup> The remarkably large grains at the top of the Pre-ST CISSe absorber are formed owing to the liquid  $\text{Na}_2\text{Se}_x$ -assisted crystallization during the selenization.<sup>[10a,13c,26]</sup> Both the reference CISSe and the PST CISSe show a similar morphology. However, larger grains are observed in PST CISSe rather than in the reference CISSe, indicating that grains can further grow by the second high-temperature step after PST.<sup>[18b,27]</sup> Simultaneously, the thickness of the fine-grained layer in PST CISSe is obviously reduced compared to the reference CISSe.

The current density–voltage ( $J$ – $V$ ) characteristics of the CISSe solar cells without/with NaCl incorporation are shown in **Figure 5**, and the corresponding device parameters are summarized in **Table 1**. The PV performance of samples selenized one time or two times is very similar compared to the changes found with Na treatment, indicating that the two-time selenization does not change the PV performance significantly (**Figure S2**, Supporting Information). Therefore, the one-time selenization reference CISSe solar cells are utilized for comparison in this research. After Na incorporation,  $j_{\text{sc}}$  of the best CISSe solar cells

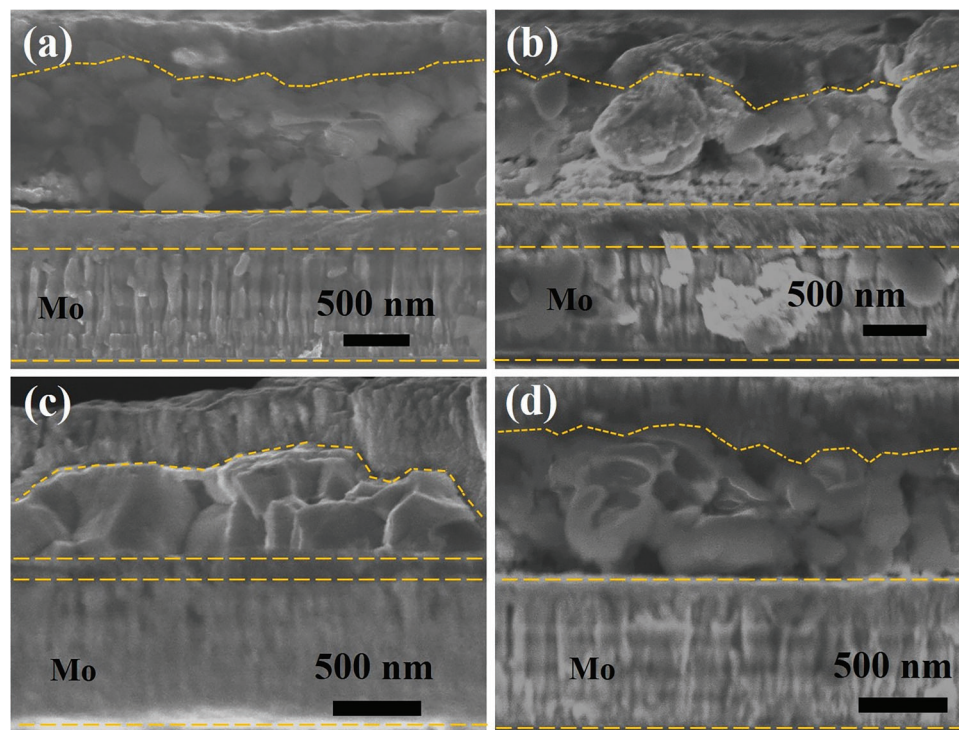


Figure 4. Cross-sectional SEM images of CISSe a) reference, b) Pre-DT, c) Pre-ST, and d) PST device.

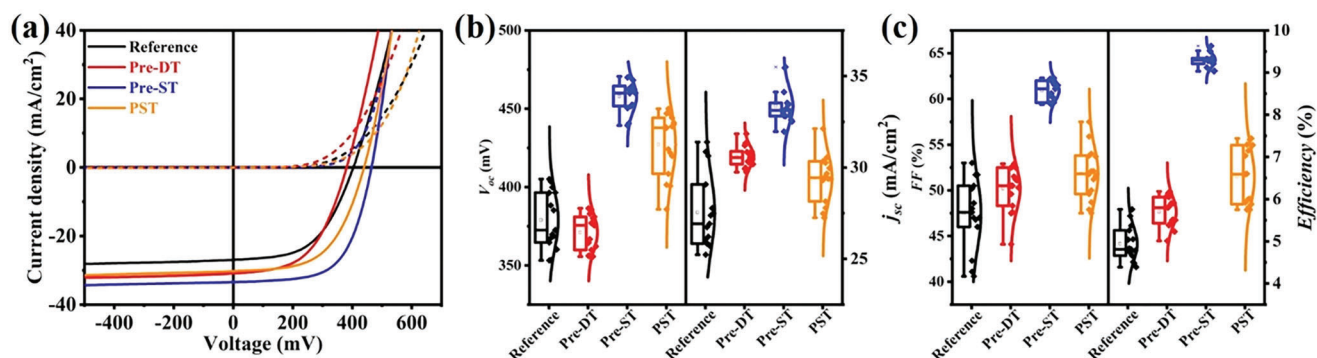


Figure 5. a)  $J$ - $V$  curves of the best CISSe solar cells without/with NaCl treatment; statistical distributions of b) open circuit voltage  $V_{oc}$  and short circuit current density  $j_{sc}$ , c) fill factor  $FF$  and efficiency derived from 15 devices without/with NaCl treatment.

Table 1. Photovoltaic performance parameters of CISSe solar cells subject to various Na incorporation strategies.

Sample	$V_{oc}$ [mV]	$j_{sc}$ [mA cm <sup>-2</sup> ]	$FF$ [%]	Efficiency [%]	$G_{sh}$ [mS cm <sup>-2</sup> ]	$R_{sh}$ [ $\Omega$ cm <sup>-2</sup> ]	$R_s$ [ $\Omega$ cm <sup>2</sup> ]	A	$j_0 \times 10^{-3}$ [mA cm <sup>-2</sup> ]
Reference	379.0 ± 18.3	27.5 ± 2.0	47.5 ± 3.8	4.9 ± 0.4	3.56 ± 1.30	300.09 ± 61.58	2.61 ± 0.34	1.94 ± 0.14	33.83 ± 28.29
	403.5	26.9	53.0	5.8	2.75	363.64	2.07	1.84	9.69
Pre-DT	371.1 ± 11.3	30.6 ± 0.6	50.2 ± 2.4	5.7 ± 0.4	3.89 ± 1.43	282.77 ± 77.05	1.83 ± 0.33	2.03 ± 0.11	60.29 ± 29.99
	381.0	30.9	52.5	6.2	3.09	323.62	1.51	1.88	24.85
Pre-ST	457.7 ± 9.7	33.4 ± 1.0	60.9 ± 1.1	9.3 ± 0.2	2.12 ± 0.37	484.48 ± 76.19	0.70 ± 0.09	2.07 ± 0.11	4.29 ± 1.84
	464.5	33.4	62.0	9.6	1.71	584.79	0.50	2.13	8.90
PST	427.2 ± 20.2	29.4 ± 1.3	51.8 ± 2.8	6.5 ± 0.7	2.61 ± 0.41	390.43 ± 52.49	1.77 ± 0.45	2.30 ± 0.23	19.57 ± 11.51
	439.9	30.3	55.9	7.4	2.33	429.18	1.13	2.17	13.12

is improved (Figure 3c).<sup>[15]</sup> The highest efficiency achieved for the reference, the Pre-DT, the Pre-ST, and the PST CISSe devices is 5.8%, 6.2%, 9.6%, and 7.4%, respectively. Comparing the best CISSe devices, the *FF* increases for Pre-ST and PST CISSe but decreases for Pre-DT CISSe compared to the reference. The decreased *FF* of the Pre-DT device can be attributed to the degraded morphology of the absorber (Figure 4b).<sup>[13c]</sup>  $V_{oc}$ ,  $j_{sc}$ , and *FF* of the highest efficient (9.6%) Pre-ST CISSe device achieve 464.5 mV, 33.4 mA cm<sup>-2</sup>, and 62.0%, respectively. This improvement in PV parameters is related to the uniform Na distribution (Figure 3) as well as to the better absorber morphology (Figure 4).

The series resistance ( $R_s$ ), the shunt resistance ( $R_{sh}$ ), the ideality factor (*A*), and the reverse saturation current density ( $j_0$ ) are calculated from the light *J*-*V* data by using the Hegedus method and are summarized in Figure S3 (Supporting Information) and Table 1.<sup>[28]</sup> Compared to the reference CISSe device, larger  $R_{sh}$  values are observed for the Pre-ST and the PST CISSe devices, whereas a smaller  $R_{sh}$  is obtained for the case of Pre-DT. The reduced  $R_{sh}$  in Pre-DT CISSe comes from the serious shunt recombination of the absorber caused by its degraded morphology (Figure 4b).<sup>[12,13c]</sup> The Na-treated CISSe devices exhibit smaller  $R_s$  values compared to the reference, indicating that Na incorporation can improve the carrier transport properties (Table 1).<sup>[15]</sup> However, larger *A* values are observed in Na-treated CISSe, indicating that the pn-junction quality becomes inferior.<sup>[15]</sup> The Cu vacancies on the surface can be occupied by Na and form Na<sub>Cu</sub> defects, which will hinder the Cd<sup>2+</sup> diffusion and formation of electrically beneficial Cd<sub>Cu</sub> donor defects during the CdS CBD process (Figure 3a).<sup>[22]</sup> The  $j_0$  of Pre-ST CISSe solar cells is smaller than for reference, Pre-DT, and PST (Table 1), implying the obvious reduction of bulk recombination in the Pre-ST CISSe absorber.<sup>[13c]</sup>

The statistical distributions of the PV parameters for 15 CISSe sub-cells of each recipe are shown in Figure 5b,c. The trends are similar to those of the corresponding highest-efficiency CISSe devices. After Na incorporation, CISSe solar cells present efficiency improvement, which is attributed to the enhancement of  $j_{sc}$  and *FF*.<sup>[13c,18b,27]</sup> The Pre-ST and the PST solar cells display an increase in  $V_{oc}$ , however, a degraded  $V_{oc}$  is observed for Pre-DT owing to the deteriorated morphology.<sup>[13c,15]</sup> The average values of  $V_{oc}$ ,  $j_{sc}$ , *FF*, and efficiency are 379.0 mV, 27.5 mA cm<sup>-2</sup>, 47.5%, 4.9%, respectively, for reference CISSe. When the Pre-ST strategy is utilized for Na incorporation, these parameters are relatively increased by 15.1%, 24.2%, 20.0%, and 65.5%, respectively (Table 1). Simultaneously, the PV parameters of Pre-ST CISSe solar cells are more uniform than for the other types, indicating that the Pre-ST is an effective strategy for PV performance improvement.

The external quantum efficiency (EQE) spectra of the CISSe devices without/with Na incorporation are shown in Figure 6a. The EQE curves are highly similar below the wavelength of 390 nm due to the identical CdS/i-ZnO/AZO top layers.<sup>[29]</sup> Obvious improvements of EQE response at wavelengths above 930 nm are observed in CISSe absorbers with Na incorporation. The improvement in EQE above 930 nm wavelength can be attributed to the higher Se and lower S concentration in the Na-treated CISSe absorbers (Figure 3c), resulting in a smaller band gap as detailed below. The Pre-ST CISSe solar cell exhibits on an average 20% higher EQE (400–1100 nm) response with a max-

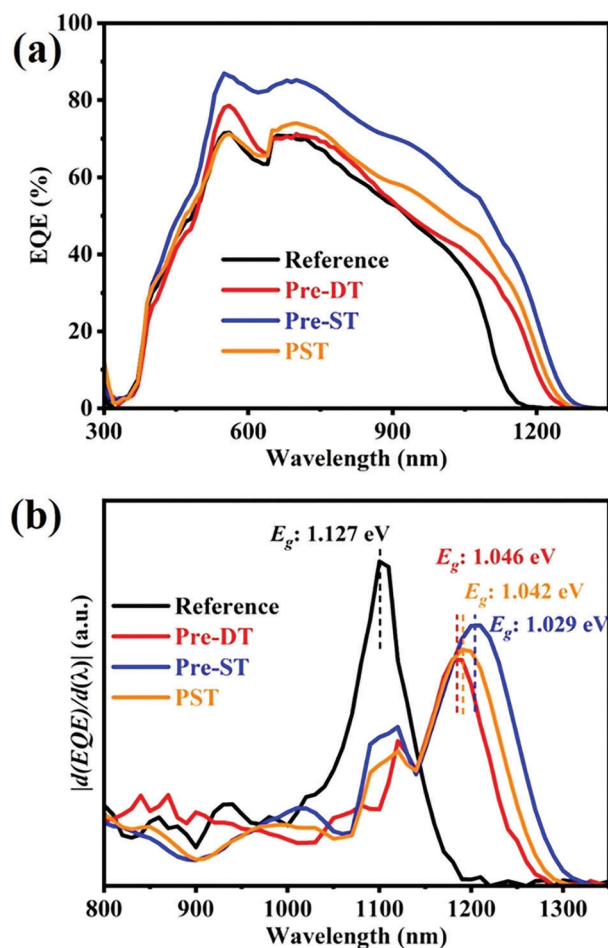


Figure 6. a) External quantum efficiency curves and b) band gap extraction for CISSe solar cells without/with Na incorporation.

imum value of 86% at 550 nm, which can be attributed to the more uniform Na concentration in the bulk as well as the better morphology compared to the other absorbers.

The band gaps ( $E_g$ ) of these CISSe absorbers are extracted from the analysis of the EQE derivative  $|d(EQE)/d\lambda|$ .<sup>[27]</sup> The reference CISSe absorber has the largest  $E_g$  (1.127 eV), which can be explained by the notably higher S concentration (Figure 3c). The CISSe absorbers with Na incorporation show similar S and Se concentrations, leading to similar  $E_g$  values (see Figure 6b and Table 2).

The acceptor doping density ( $N_A$ ) and the width of the depletion region ( $W_d$ ) of CISSe solar cells of each type are extracted from the room temperature *C*-*V* profiles (Figure 7a) by the following equations:<sup>[16a,22a]</sup>

$$\frac{1}{C^2} = \frac{2}{q\epsilon_0\epsilon_R N_A} V = \frac{2}{q\epsilon_0\epsilon_R N_A} (V_{bi} - V_{app}) \quad (2)$$

$$W_d = \frac{\epsilon_0\epsilon_R A}{C} \quad (3)$$

where *C* and *A* stand for the measured capacitance and the active area of the device,  $q$ ,  $\epsilon_0$ ,  $\epsilon_R$ ,  $V_{bi}$ , and  $V_{app}$  represent the elemen-

**Table 2.** Electrical parameters of the best-efficient CISSe devices without/with Na incorporation.

Sample	$E_g$ [eV]	$V_{oc,def}$ [mV]	$N_A \times 10^{15}$ [cm <sup>-3</sup> ]	$W_d$ [nm]	$E_{a1}$ [eV]	$E_{a2}$ [eV]	$\Phi_B$ [eV]
Reference	$1.096 \pm 0.039$	$717.5 \pm 22.5$	$9.0 \pm 4.9$	$542.1 \pm 53.1$	1.079	0.738	0.341
	1.127	723.5	6.3	552.4			
Pre-DT	$1.046 \pm 0.004$	$675.2 \pm 13.3$	$10.3 \pm 1.9$	$493.1 \pm 37.5$	1.007	0.689	0.318
	1.046	665.0	7.5	499.5			
Pre-ST	$1.029 \pm 0.005$	$572.2 \pm 8.8$	$7.9 \pm 2.9$	$361.6 \pm 45.9$	1.036	0.819	0.217
	1.029	564.5	4.6	437.5			
PST	$1.042 \pm 0.011$	$615.1 \pm 28.6$	$24.0 \pm 11.9$	$338.4 \pm 21.0$	1.048	0.773	0.275
	1.042	602.1	11.9	341.7			

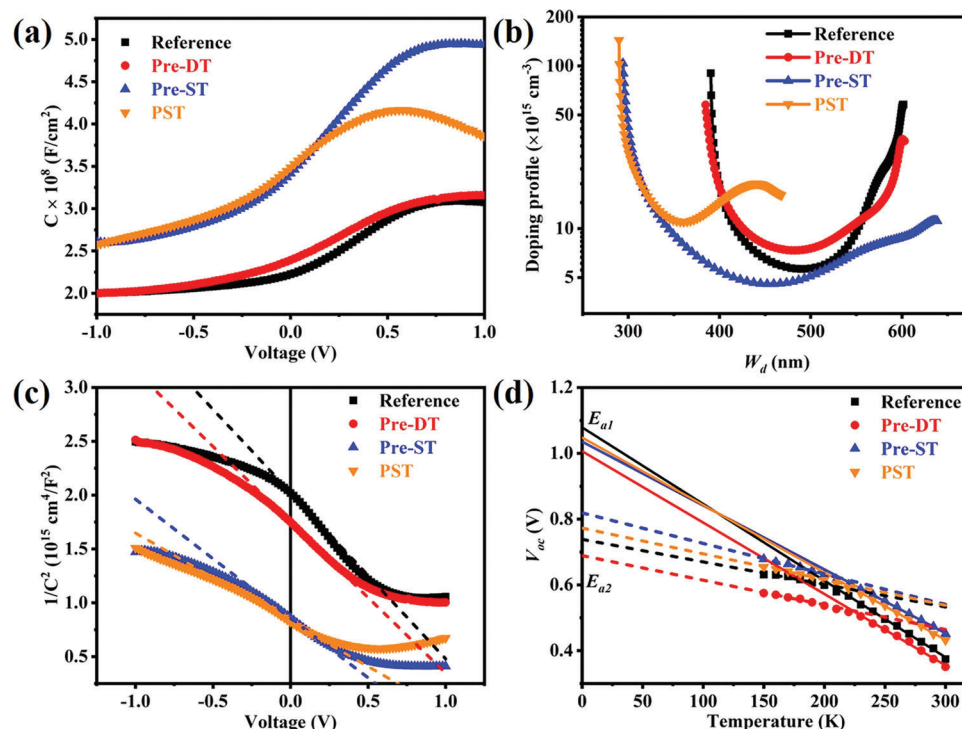


**Figure 7.** a) C–V curves, b) doping profiles, c) Mott–Schottky plot of  $1/C^2$  versus  $V$ , and d) temperature-dependent open-circuit voltage of CISSe solar cells without/with NaCl incorporation.

tary charge, the permittivity in vacuum, the dielectric constant of CISSe, the built-in voltage, and the applied voltage.  $N_A$  and  $W_d$  are extracted from the forward bias voltage (equation 2) and at 0 bias voltage (equation 3), respectively.

For the reference CISSe solar cell, an  $N_A$  of  $6.3 \times 10^{15} \text{ cm}^{-3}$  and a  $W_d$  of 522.4 nm are found (Figure 7b). These results indicate that  $N_A$  is affected by the defect concentration owing to a great number of Cu vacancies (Cu-poor absorber, Figure 3b). In other words, the  $N_A$  value is influenced by the Na-doping level and the defect concentration. The Pre-DT CISSe and the PST CISSe solar cell present an increase in  $N_A$ , whereas a smaller value is observed for the Pre-ST CISSe device (see Figure 7c, S3, Supporting Information, and Table 2). The morphology of the absorber can also affect the result of CV measurement.<sup>[15]</sup> The pronounced low value of  $N_A$  for Pre-ST CISSe can be attributed to the large-grained absorber with a small number of grain boundaries. With Na incorporation, the  $\text{Na}_{\text{Cu}}$  defect will form on the

surface of CISSe absorbers, hindering the  $\text{Cd}^{2+}$  diffusion during the CdS CBD process.<sup>[15,22b]</sup> Therefore, with increasing the Na concentration, the  $W_d$  value of the corresponding solar cells decreases. This is most pronounced for Na addition on the top of the precursor/absorber layer.

Alkali treatment can significantly reduce the open circuit-voltage deficit  $V_{oc,def}$  owing to the improvement in absorber quality and the decrease in carrier recombination.<sup>[14,30]</sup>  $V_{oc,def}$  is defined as  $E_g/q - V_{oc}$ , where  $q$  is the elementary charge.<sup>[14,24]</sup> After Na incorporation, the  $V_{oc,def}$  can be significantly reduced (Figure S4, Supporting Information and Table 2).

The Urbach energy ( $E_U$ ) is a further indicator of the semiconductor quality, which has been utilized to evaluate the performance of the solar cell.<sup>[30,31]</sup> After Na incorporation,  $E_U$  reduces from 21.67 meV for the reference CISSe to 17.19 meV for the Pre-DT CISSe, 16.20 meV for the Pre-ST CISSe, and 14.86 meV for the PST CISSe (Figure S5, Supporting Information). The reduced

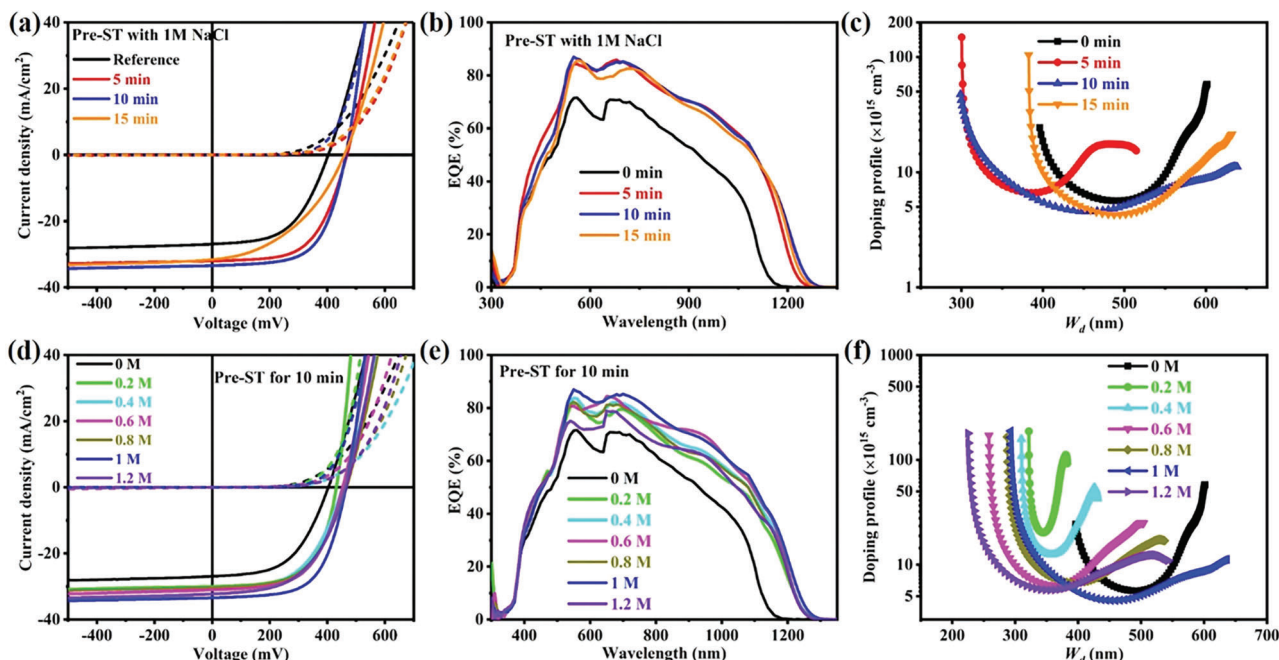


**Figure 8.** a)  $J$ - $V$  curves, b) EQE spectra, and c) doping profiles of CISSe with various times of pre-selenization treatment in 1 M NaCl solution. d)  $J$ - $V$  curves, e) EQE spectra, and f) doping profiles of CISSe fabricated with various NaCl concentrations for 10 min pre-selenization treatment.

$E_U$  reflects better carrier transport and less carrier recombination in the Na-treated CISSe solar cells.<sup>[14,30]</sup>

There are two recombination paths in the CISSe solar cells: interface recombination and bulk recombination. Temperature-dependent open-circuit voltage (IVT) measurements are an effective technique to evaluate the dominant recombination mechanism. The activation energy ( $E_a$ ) is extracted from the IVT profile by linear extrapolation to  $T = 0$  K via the following formula:<sup>[21]</sup>

$$V_{oc} = \frac{E_a}{q} - \frac{AkT}{q} \ln \left( \frac{j_{00}}{j_{sc}} \right) \quad (4)$$

where  $E_a$ ,  $A$ ,  $k$ , and  $j_{00}$  are the activation energy of the dominant recombination mechanism, the diode ideality factor, the Boltzmann constant, and the reverse saturation current density, respectively. Two extrapolated values are obtained from slope fitting in the high and low-temperature regime, respectively:  $E_{a1}$  ( $230 \text{ K} < T < 300 \text{ K}$ ) and  $E_{a2}$  ( $150 \text{ K} < T < 200 \text{ K}$ ) (Figur). The small differences between  $E_g$  and  $E_{a1}$  are 0.048, 0.039, 0.007, and 0.006 eV, for reference, Pre-DT, Pre-ST, and PST CISSe, respectively, indicating that the dominant recombination occurs in the absorber bulk.<sup>[21]</sup> The back barrier height ( $\Phi_B$ ) can be calculated as the difference between  $E_{a1}$  and  $E_{a2}$ , and drops from  $>0.3$  eV for the reference to close to 0.2 eV for Pre-ST CISSe (Table 2).<sup>[32]</sup> Na will also incorporate into the Mo back contact, which is beneficial for Mo(S,Se)<sub>2</sub> layer formation, resulting in the reduction of the  $\Phi_B$ .<sup>[15,32b]</sup>

## 2.2. Effect of Pre-Selenization Treatment Times and NaCl Concentrations

The content of incorporated Na affects the chalcopyrite solar cell performance.<sup>[13c,15,16,25a]</sup> In our case, there are two paths to ad-

just the Na content, namely various soaking times and changing concentrations of the NaCl aqueous-ethanol solution. Based on the above discussion (Figure 5), Pre-ST for Na incorporation is the most promising strategy for performance improvement. Therefore, Pre-ST is utilized for investigating the effect of different NaCl content and the precursor films are soaked either in 1 M NaCl for various times, or in various NaCl solution concentrations for 10 min.

The  $J$ - $V$  curves of CISSe solar cells with 1 M NaCl pre-selenization treatment for various times are shown in Figure 8a. The corresponding PV parameters are detailed in Figure S6 (Supporting Information) and are summarized in Table 3. For all investigated soaking times, both  $j_{sc}$  and  $V_{oc}$  increase significantly. When the CISSe precursor films are soaked for 5 min, the highest average  $V_{oc}$  values are obtained amongst these CISSe solar cells without/with 1 M NaCl treatment, indicating that a short NaCl treatment time is beneficial for  $V_{oc}$  improvement. With prolonging the soaking time,  $j_{sc}$  firstly increases and then decreases with the maximum reached for 10 min ( $33.4 \text{ mA cm}^{-2}$  on average).  $FF$  and  $j_{sc}$  show a similar trend, with an initial increase toward the maximum for 10 min NaCl treatment and a subsequent decrease. Significantly low  $FF$  values (32.9% on average) are observed for the CISSe solar cells with 15 min NaCl treatment, leading to the remarkably low efficiencies obtained. The low efficiencies are attributed to the degradation of the CISSe grain size owing to the high concentration of  $\text{Cl}^-$  ions.<sup>[15]</sup> The Se content is crucial for removing  $\text{Cl}^-$  ions via formation of  $\text{SeCl}_6$ , similar to removing the  $\text{F}^-$  ions (from NaF) by forming  $\text{SeF}_6$  vapor.<sup>[22a,25]</sup> In our research, an equal content of Se is utilized for all selenization processes. For precursor films with longer NaCl soaking times, the Se content thus cannot support the full removal of the  $\text{Cl}^-$  ions. This reason can also explain that the highest  $V_{oc}$  values are obtained from the precursor films for short NaCl treatment time

**Table 3.** Photovoltaic performance parameters of CISSe solar cells with 1 M NaCl solution pre-selenization treatment for various times (15 sub-cells for each recipe).

Treatment time	$V_{oc}$ [mV]	$j_{sc}$ [mA cm <sup>-2</sup> ]	$FF$ [%]	Efficiency [%]	$E_g$ [eV]	$V_{oc,def}$ [mV]	$N_A \times 10^{15}$ [cm <sup>-3</sup> ]	$W_d$ [nm]
Reference	379.0 ± 18.3	27.5 ± 2.0	47.5 ± 3.8	4.9 ± 0.4	1.096 ± 0.039	717.5 ± 22.5	9.0 ± 4.9	542.1 ± 53.1
	403.5	26.9	53.0	5.8	1.127	723.5	6.3	552.4
5 min	479.1 ± 8.6	30.5 ± 1.7	57.0 ± 2.4	8.3 ± 0.3	1.048 ± 0.003	569.4 ± 9.0	7.8 ± 1.7	406.2 ± 19.7
	468.4	32.0	58.7	8.8	1.051	582.6	9.7	434.4
10 min	457.7 ± 9.7	33.4 ± 1.0	60.9 ± 1.1	9.3 ± 0.2	1.029 ± 0.005	572.2 ± 8.8	7.9 ± 2.9	361.6 ± 45.9
	464.5	33.4	62.0	9.6	1.029	564.5	4.6	437.5
15 min	451.1 ± 15.2	29.7 ± 1.7	36.9 ± 2.5	5.0 ± 0.6	1.036 ± 0.006	584.9 ± 17.7	8.7 ± 5.3	423.7 ± 51.2
	459.9	31.6	42.3	6.2	1.039	579.1	4.3	487.4

**Table 4.** Photovoltaic performance parameters of CISSe solar cells with various concentrations of NaCl solution pre-selenization treatment for various times (15 sub-cells for each recipe).

NaCl concentration	$V_{oc}$ [mV]	$j_{sc}$ [mA cm <sup>-2</sup> ]	$FF$ [%]	Efficiency [%]	$E_g$ [eV]	$V_{oc,def}$ [mV]	$N_A \times 10^{15}$ [cm <sup>-3</sup> ]	$W_d$ [nm]
Reference	379.0 ± 18.3	27.5 ± 2.0	47.5 ± 3.8	4.9 ± 0.4	1.096 ± 0.039	717.5 ± 22.5	9.0 ± 4.9	542.1 ± 53.1
	403.5	26.9	53.0	5.8	1.127	723.5	6.3	552.4
0.2 M	412.2 ± 27.4	27.8 ± 1.0	45.7 ± 6.4	5.3 ± 1.0	1.048 ± 0.008	596.3 ± 29.4	35.8 ± 14.6	349.8 ± 14.6
	431.3	30.0	58.9	7.6	1.042	610.7	28.5	360.2
0.4 M	420.3 ± 25.9	28.3 ± 1.7	38.7 ± 8.6	4.7 ± 1.4	1.034 ± 0.0066	580.0 ± 27.7	20.6 ± 8.6	374.8 ± 30.3
	452.6	30.4	54.6	7.5	1.034	581.4	15.6	380.9
0.6 M	430.3 ± 32.4	30.5 ± 2.0	49.8 ± 6.2	6.6 ± 1.1	1.038 ± 0.005	570.1 ± 32.9	19.3 ± 11.2	352.8 ± 48.6
	453.0	31.1	57.8	8.1	1.039	586.0	7.13	393.6
0.8 M	464.8 ± 4.9	29.5 ± 0.8	50.8 ± 4.0	7.0 ± 0.7	1.039 ± 0.004	538.7 ± 7.1	7.3 ± 1.5	396.6 ± 24.2
	467.1	30.3	55.5	7.8	1.036	568.9	6.7	399.1
1 M	457.7 ± 9.7	33.4 ± 1.0	60.9 ± 1.1	9.3 ± 0.2	1.029 ± 0.005	572.2 ± 8.8	7.9 ± 2.9	361.6 ± 45.9
	464.5	33.4	62.0	9.6	1.029	564.5	4.6	437.5
1.2 M	450.8 ± 11.5	30.1 ± 1.2	49.7 ± 2.9	6.8 ± 0.7	1.038 ± 0.005	586.7 ± 9.7	8.5 ± 3.2	375.2 ± 34.9
	462.3	32.3	53.7	8.0	1.037	574.7	5.8	370.2

(Se excess). After optimization of the soaking time of the precursor films (1 M NaCl for 10 min), the best CISSe device achieves 9.6% with a  $V_{oc}$  of 464.5 mV, a  $j_{sc}$  of 33.4 mA cm<sup>-2</sup>, and a  $FF$  of 62.0%.

After Na incorporation, the CISSe absorbers present a significant improvement in photoelectric response intensity in the visible and infrared wavelength ranges ( $\lambda > 450$  nm) (Figure 8b). The improvement implies better collection capability of the photo-generated carriers, which is caused by a better absorber quality with fewer defects. Simultaneously, NaCl-treated CISSe absorbers have a smaller  $E_g$  value than the reference CISSe due to the smaller S content (Figure S7, Supporting Information and Table 3). The Na will bond with Se to form a Na<sub>2</sub>Se<sub>x</sub> liquid compound, which can assist the Se diffusion during the high-temperature selenization.<sup>[10a,13c]</sup> Therefore, the substitution of S by Se in Na-treated CISSe absorber is higher than in the reference CISSe, leading to better CISSe absorber quality and better EQE response.<sup>[15]</sup> Again, smaller values of  $W_d$  arise with NaCl treatment because the Na<sub>Cu</sub> defect formation at the CISSe surface hinders the Cd<sup>2+</sup> diffusion, reducing the width of the space charge region (Figure 8c).<sup>[15,22]</sup>  $N_A$  is affected by the amount of

Na in the absorber and by its morphology.<sup>[15]</sup> With prolonging the precursor soaking time,  $N_A$  firstly increases then decreases, in accordance with literature results for solution-processed chalcopyrite solar cells (Figure 8c).<sup>[15,33]</sup> The statistics of  $N_A$ ,  $W_d$ ,  $E_g$ , and  $V_{oc,def}$  are presented in Figure S8 (Supporting Information) and are summarized in Table 3. Thanks to the increase in  $V_{oc}$  and the reduction of  $E_g$  after Na incorporation, the  $V_{oc,def}$  values are remarkably reduced (Figure S8, Supporting Information and Table 3).

The concentration of the NaCl solution can strongly affect the properties of CISSe solar cells.<sup>[13c]</sup> The  $J$ - $V$  curves of the best CISSe solar cells subject to Pre-ST in various concentrations of NaCl for 10 min are shown in Figure 8d and Table 4. The statistics of the PV parameters of these solar cells are presented in Figure S9 (Supporting Information) and reveal a significant improvement of  $V_{oc}$ ,  $j_{sc}$ ,  $FF$ , and efficiency after Na incorporation. With increasing the concentration of the NaCl solution from 0 to 1.2 M, the PV parameters first improve and then degrade with the highest  $V_{oc}$  value observed for 0.8 M NaCl, and the highest  $j_{sc}$  and  $FF$  for 1 M NaCl. Therefore, the champion efficiency of 9.6% with a  $V_{oc}$  of 464.5 mV, a  $j_{sc}$  of 33.4 mA cm<sup>-2</sup>, and a  $FF$  of



62.0% remains at 1 M NaCl Pre-ST for 10 min. The EQE curves of these CISSe solar cells with various concentrations of NaCl for 10 min Pre-ST significantly improve in the wavelength range above 400 nm compared to the Na-free reference (Figure 8e). The possible explanation also here may be a better CISSe absorber quality with fewer defects after Na incorporation, leading to better photoelectric response and separation of photo-generated hole–electron pairs.<sup>[13c,15]</sup> It is one of the reason for the  $j_{sc}$  improvement obtained from the  $J$ – $V$  measurement. Compared to the reference CISSe solar cell, Na-treated CISSe solar cells present higher EQE responses (Figure 8e) and narrower  $E_g$  values (Figure S10, Supporting Information). These results are similar to the results of precursor films with various soaking times in 1 M NaCl solution (Figure 6). The solar cell with 1 M NaCl treatment exhibits over 20% (on average) higher EQE (400–1000 nm) and the maximum EQE value achieves 88.7% at 550 nm wavelength. Simultaneously, the Na-treated CISSe absorbers have higher EQE responses at wavelengths above 1020 nm than the reference CISSe (Figure 8e). These results are in good agreement with the outstanding  $j_{sc}$  of 1 M NaCl Pre-ST CISSe solar cells (Table 4). Compared to the reference CISSe solar cells, the average values of  $N_A$  firstly increase until the NaCl concentration reaches 0.2 M and then decrease for higher NaCl concentration (Figure S11, Supporting Information). On the contrary, NaCl-treated CISSe solar cells have a narrower  $W_d$  than the reference CISSe solar cells (Figure 8f and Figure S11, Supporting Information). After Na incorporation, the  $V_{oc,def}$  values are in general significantly reduced owing to better CISSe absorber quality (Figure S11, Supporting Information and Table 4). In sum, the highest efficient CISSe solar cells are fabricated from the solution-processed precursor films with 1 M NaCl aqueous-ethanol solution Pre-ST for 10 min.

### 3. Conclusion

We have investigated the PV performance improvement of solution-processed CISSe solar cells by using NaCl aqueous-ethanol solution for Na incorporation. The Na-treated CISSe absorbers present significantly lower S content, resulting in narrower band gaps and  $j_{sc}$  improvement. For the Pre-ST (adding Na before selenization), the CISSe absorbers exhibit a uniform Na distribution and large grains. The Pre-ST CISSe solar cells achieve better PV performances than for Pre-DT (Na deposition before spin-coating of precursor solution) or PST (addition of Na after selenization). Additionally, Na-treated CISSe solar cells have lower  $V_{oc,def}$  and  $\Phi_B$  compared to the reference CISSe. The Na content can be adjusted by the soaking time of the precursor films or the concentration of NaCl solution. The optimal strategy in our research is to soak the precursor films (Pre-ST) in 1 M NaCl solution for 10 min. The highest efficiency achieved is 9.6% with  $V_{oc}$  of 464.5 mV,  $j_{sc}$  of 33.4 mA cm<sup>-2</sup>, and FF of 62.0%. Compared to the reference CISSe, the  $V_{oc}$ ,  $j_{sc}$ , FF, and efficiency of the highest efficient Pre-ST CISSe device are improved relatively by 15.1%, 24.2%, 20.0%, and 65.5%. The  $V_{oc,def}$  decreases from 704.5 to 551.5 mV and the back barrier height from 0.341 to 0.217 eV, underlining the improvement by adequate Na treatment. The Pre-ST for Na incorporation is a promising strategy for efficiency improvement of solution-processed chalcopyrite solar cells.

### 4. Experimental Section

**Preparation of Cu-In-TU-DMF Precursor Solution:** 34.5 mmol of TU was first added in 16 mL DMF solvent with stirring vigorously until a clear TU-DMF solution formed. Following, 5.1 mmol CuCl was completely dissolved in the previous TU-DMF solution under severe stirring. To obtain a Cu-poor molecular precursor solution, 5.5 mmol InCl<sub>3</sub> was added, and a yellowish solution (Cu-In-TU-DMF solution) was obtained after overnight stirring. Finally, the solution was filtered by using a 0.45 μm polytetrafluoroethylene filter.

**Preparation of CISSe Absorber:** The precursor solution was spin-coated at 1500 rpm for 60 s onto an 800 nm thick Mo layer separated from the glass substrate by a Si<sub>3</sub>N<sub>4</sub> barrier. Then the wet film was immediately annealed on a hot plate at 350 °C for 2 min and moved to a ceramic plate for cooling down naturally. The coating-annealing-cooling cycle was repeated 8 times to obtain a total film thickness of around 820 nm. The as-prepared Cu-In-S precursor films were processed in a tube furnace under Ar atmosphere with 250 mg Se powder for 2 samples (2.5 × 2.5 cm<sup>2</sup>) by a first annealing step at 350 °C for 15 min and a second step at 540 °C for 20 min to form the CISSe absorber.

To research the effect of Na incorporation strategies, 1 M NaCl aqueous-ethanol solution (volume ratio of ultra-pure water to ethanol is 1:1) was utilized for Na incorporation. NaCl was introduced in various experiment stages (Figure 1): either prior to absorber deposition (pre-deposition treatment, Pre-DT), before selenization (pre-selenization treatment, Pre-ST), or after selenization (post-selenization treatment, PST). For the Pre-DT, the Mo back contact was soaked in 1 M NaCl for 10 min and then dried in N<sub>2</sub> flow. After that, the precursor film was deposited on the treated Mo back contact and subject to selenization, just as the reference sample. For the Pre-ST, the as-deposited precursor film was soaked in 1 M NaCl solution for 10 min and then dried in N<sub>2</sub> flow. The selenization process of the Pre-ST film was identical to the reference sample. For the PST, a sample of reference type was soaked in 1 M NaCl solution for 10 min, dried in N<sub>2</sub> flow, and annealed in 250 mg Se powder for 2 samples at 540 °C for 20 min.

To research the effect of treatment times of Pre-ST, the precursor films were soaked in 1 M NaCl solution for 5, 10, and 15 min. These Na-doped precursor films were subject to selenization under the same conditions as the reference sample.

To research the effect of NaCl concentration on the Pre-ST, a concentration range from 0.2 to 1.2 M with a step of 0.2 M was researched. The soaking time was 10 min, then the samples were dried in N<sub>2</sub> gas flow. Following, the selenization was identical to the reference sample.

**Fabrication of CISSe Solar Cells:** A 10% KCN solution was utilized for removing Cu<sub>2-x</sub>Se and excessive Se of the absorbers. Then, an 80 nm CdS buffer layer was coated by chemical bath deposition. Afterward, an 80 nm/300 nm i-ZnO/Al:ZnO(AZO) bi-layer was sputtered successively. Finally, a Ni/Al top grid was deposited by thermal evaporation. The active area of each CISSe solar cell was determined to be 0.5 cm<sup>2</sup> by mechanical scribing.

**Characterization:** The composition profiles of the films were measured by using a GD-OES (glow discharge optical emission spectroscopy) spectrometer GDA 650 HR analyzer of Spectrumba. A home-built Raman system by Femtika was employed for Raman scattering measurement with an excitation laser of 532 nm wavelength. For the GDOES and Raman measurement, the CdS/i-ZnO/AZO/Ni/Al layers were removed from the top of finished solar cells by 10% HCl etching to release the absorber. Morphologies of the PV devices were measured by scanning electron microscopy (SEM) using a JEOL JSM-7500F. The current density–voltage ( $J$ – $V$ ) curves were measured under standard test conditions (AM1.5G; 100 mW cm<sup>-2</sup>; 25 °C) by a WACOM sun-simulator containing both a Xenon and a Halogen lamp. The external quantum efficiency (EQE) measurements were performed with a self-built EQE setup calibrated in the wavelength range of 300–1350 nm with Si and Ge diodes as references. For the capacitance–voltage ( $C$ – $V$ ) measurements, a BK PRECISION Model 895 operated at 100 kHz was utilized with a 5 mV testing signal in dark conditions. In addition, the temperature-dependent current density–voltage measurements were carried out in an enclosed

liquid helium cryostat with the temperature sensor mounted atop the sample.

## Supporting Information

Supporting Information is available from the Wiley Online Library or from the author.

## Acknowledgements

The authors would like to thank Klaus Pärshcke for the window layer and front contact deposition, and Ihab Kardosh for performing the Raman measurement. The authors acknowledge Jeldrik Schulte, AG Winterer (UDE) for support with SEM measurements. The XRF and GDOES measurements were performed on an instrument funded by the Deutsche Forschungsgemeinschaft (DFG, German Research Foundation)—INST 20876/324-1 FUGG and are acknowledged as follows: “Gefördert durch die Deutsche Forschungsgemeinschaft (DFG)—Projektnummer INST 20876/324-1 FUGG.” The Raman measurements were performed on a Next-Gen Cluster-Tool funded by the Deutsche Forschungsgemeinschaft (DFG, German Research Foundation)—INST 20876/347-1 FUGG and are acknowledged as follows: “Gefördert durch die Deutsche Forschungsgemeinschaft (DFG)—Projektnummer INST 20876/347-1 FUGG.” Y.G. especially acknowledges the financial support of the Chinese Scholarship Committee, and G.Y. the funding from the National Natural Science Foundation of China (NSFC, 51802240) and the funding support of the Fundamental Research Funds for the Central Universities (WUT:183101002, 193201003). The authors acknowledge support from the Open Access Publication Fund of the University of Duisburg-Essen.

Open access funding enabled and organized by Projekt DEAL.

## Conflict of Interest

The authors declare no conflict of interest.

## Data Availability Statement

The data that support the findings of this study are available from the corresponding author upon reasonable request.

## Keywords

ClSSe, NaCl aqueous-ethanol solution, Na incorporation, pre-selenization treatment, solution process

Received: March 27, 2023  
Revised: June 1, 2023  
Published online:

- [1] M. Nakamura, K. Yamaguchi, Y. Kimoto, Y. Yasaki, T. Kato, H. Sugimoto, *IEEE J. Photovolt.* **2019**, *9*, 1863.
- [2] a) K. F. Tai, R. Kamada, T. Yagioka, T. Kato, H. Sugimoto, *Jpn. J. Appl. Phys.* **2017**, *56*, 08MC03; b) T. Kato, *Jpn. J. Appl. Phys.* **2017**, *56*, 030307; c) T.-Y. Lin, I. Khatri, J. Matsuura, K. Shudo, W.-C. Huang, M. Sugiyama, C.-H. Lai, T. Nakada, *Nano Energy* **2020**, *68*, 104299.
- [3] S. Suresh, A. R. Uhl, *Adv. Energy Mater.* **2021**, *11*, 2003743.
- [4] T. Zhang, Y. Yang, D. Liu, S. C. Tse, W. Cao, Z. Feng, S. Chen, L. Qian, *Environ. Sci.* **2016**, *9*, 3674.
- [5] C.-H. Chung, K.-H. Hong, D.-K. Lee, J. H. Yun, Y. Yang, *Chem. Mater.* **2015**, *27*, 7244.
- [6] G. S. Park, V. B. Chu, B. W. Kim, D. W. Kim, H. S. Oh, Y. J. Hwang, B. K. Min, *ACS Appl. Mater. Interfaces* **2018**, *10*, 9894.
- [7] T. Aramoto, Y. Kawaguchi, Y.-C. Liao, Y. Kikuchi, T. Ohashi, H. Iida, A. Nakamura, presented at 32nd European Photovoltaic Solar Energy Conf. and Exhibition, Munich, Germany, June **2016**, p. 1108.
- [8] A. R. Uhl, J. K. Katahara, H. W. Hillhouse, *Environ. Sci.* **2016**, *9*, 130.
- [9] J. A. Clark, A. Murray, J. M. Lee, T. S. Autrey, A. D. Collord, H. W. Hillhouse, *J. Am. Chem. Soc.* **2019**, *141*, 298.
- [10] a) J. Jiang, R. Giridharagopal, E. Jedlicka, K. Sun, S. Yu, S. Wu, Y. Gong, W. Yan, D. S. Ginger, M. A. Green, X. Hao, W. Huang, H. Xin, *Nano Energy* **2020**, *69*, 104438; b) J. Jiang, S. Yu, Y. Gong, W. Yan, R. Zhang, S. Liu, W. Huang, H. Xin, *Sol. RRL* **2018**, *2*, 1800044.
- [11] a) C. van Lare, G. Yin, A. Polman, M. Schmid, *ACS Nano* **2015**, *9*, 9603; b) G. Yin, M. W. Knight, M.-C. van Lare, M. M. Solà Garcia, A. Polman, M. Schmid, *Adv. Opt. Mater.* **2017**, *5*, 1600637; c) G. Yin, V. Brackmann, V. Hoffmann, M. Schmid, *Sol. Energy Mater. Sol. Cells* **2015**, *132*, 142; d) G. Yin, M. Song, M. Schmid, *Sol. Energy Mater. Sol. Cells* **2019**, *195*, 318.
- [12] Y. Kong, L. Huang, Z. Chi, X. Wu, J. Li, X. Xiao, *ACS Appl. Mater. Interfaces* **2020**, *12*, 52857.
- [13] a) Y. Wang, S. Lv, Z. Li, *J. Mater. Sci. Technol.* **2022**, *96*, 179; b) K. Kim, I. Jeong, Y. Cho, D. Shin, S. Song, S. K. Ahn, Y.-J. Eo, A. Cho, C. Jung, W. Jo, J. H. Kim, P.-P. Choi, J. Gwak, J. H. Yun, *Nano Energy* **2020**, *67*, 104201; c) S. Rehan, J. Moon, T. G. Kim, J. Gwak, J. Kim, J. W. Kim, W. Jo, S. K. Ahn, S. Ahn, *Nano Energy* **2018**, *48*, 401; d) P. Schöppe, S. Schönherr, M. Chugh, H. Mirhosseini, P. Jackson, R. Wuerz, M. Ritzer, A. Johannes, G. Martínez-Criado, W. Wisniewski, T. Schwarz, C. T. Plass, M. Hafermann, T. D. Kühne, C. S. Schnohr, C. Ronning, *Nano Energy* **2020**, *71*, 104622.
- [14] J. Chantana, Y. Kawano, T. Nishimura, Y. Kimoto, T. Kato, H. Sugimoto, T. Minemoto, *ACS Appl. Energy Mater.* **2020**, *3*, 1292.
- [15] S. Uličná, L. M. Welch, A. Abbas, M. Togay, V. Tsai, T. R. Betts, A. V. Malkov, J. M. Walls, J. W. Bowers, *Prog. Photovoltaics* **2021**, *29*, 546.
- [16] a) Y. Li, G. Yin, Y. Gao, T. Köhler, J. Lucaßen, M. Schmid, *Sol. Energy Mater. Sol. Cells* **2021**, *223*, 110969; b) Y.-C. Lin, D.-H. Hong, Y.-T. Hsieh, L.-C. Wang, H.-R. Hsu, *Sol. Energy Mater. Sol. Cells* **2016**, *155*, 226; c) T.-Y. Lin, C.-H. Chen, L.-W. Wang, W.-C. Huang, Y.-W. Jheng, C.-H. Lai, *Nano Energy* **2017**, *41*, 697.
- [17] a) R. Carron, S. Nishiwaki, T. Feurer, R. Hertwig, E. Avancini, J. Löckinger, S.-C. Yang, S. Buecheler, A. N. Tiwari, *Adv. Energy Mater.* **2019**, *9*, 1900408; b) R. Caballero, C. A. Kaufmann, T. Eisenbarth, A. Grimm, I. Laueremann, T. Unold, R. Klenk, H. W. Schock, *Appl. Phys. Lett.* **2010**, *96*, 092104.
- [18] a) U. Berner, D. Colombara, J. de Wild, E. V. C. Robert, M. Schütze, F. Hergert, N. Valle, M. Widenmeyer, P. J. Dale, *Prog. Photovoltaics* **2016**, *24*, 749; b) Q. Guo, G. M. Ford, R. Agrawal, H. W. Hillhouse, *Prog. Photovoltaics* **2013**, *21*, 64.
- [19] S. Yu, Y. Gong, J. Jiang, S. Wu, W. Yan, X. Li, W. Huang, H. Xin, *Sol. RRL* **2019**, *3*, 190052.
- [20] a) Y.-T. Yen, Y.-C. Wang, Y.-Z. C. Chen, H.-W. Tsai, F. Hu, S.-M. Lin, Y.-J. Chen, C.-C. Lai, W. Liu, T.-H. Wang, H.-F. Hong, Y.-L. Chueh, *ACS Appl. Mater. Interfaces* **2014**, *6*, 8327; b) S. Wu, J. Jiang, S. Yu, Y. Gong, W. Yan, H. Xin, W. Huang, *Nano Energy* **2019**, *62*, 818.
- [21] X. Lin, R. Klenk, L. Wang, T. Köhler, J. Albert, S. Fiechter, A. Ennaoui, M. C. Lux-Steiner, *Environ. Sci.* **2016**, *9*, 2037.
- [22] a) B. Duan, L. Guo, Q. Yu, J. Shi, H. Wu, Y. Luo, D. Li, S. Wu, Z. Zheng, Q. Meng, *J. Energy Chem.* **2020**, *40*, 196; b) F. Pianezzi, P. Reinhard, A. Chirilă, B. Bissig, S. Nishiwaki, S. Buecheler, A. N. Tiwari, *Phys. Chem. Chem. Phys.* **2014**, *16*, 8843.
- [23] O. Cojocaru-Miréidin, E. Ghorbani, M. Raghuvanshi, X. Jin, D. Pandav, J. Keutgen, R. Schneider, D. Gerthsen, K. Albe, R. Scheer, *Nano Energy* **2021**, *89*, 106375.

- [24] S. Yu, B. Li, J. Jiang, X. Liu, S. Hao, S. Han, W. Yan, H. Xin, *Adv. Energy Mater.* **2021**, *12*, 2103644.
- [25] a) Y. Sun, S. Lin, W. Li, S. Cheng, Y. Zhang, Y. Liu, W. Liu, *Engineering* **2017**, *3*, 452; b) A. Laemmle, R. Wuerz, T. Schwarz, O. Cojocar-Mirédin, P.-P. Choi, M. Powalla, *J. Appl. Phys.* **2014**, *115*, 154501.
- [26] Y. E. Romanyuk, H. Hagendorfer, P. Stücheli, P. Fuchs, A. R. Uhl, C. M. Sutter-Fella, M. Werner, S. Haass, J. Stükelberger, C. Broussillou, P.-P. Grand, V. Bermudez, A. N. Tiwari, *Adv. Funct. Mater.* **2015**, *25*, 12.
- [27] S. M. McLeod, C. J. Hages, N. J. Carter, R. Agrawal, *Prog. Photovoltaics* **2015**, *23*, 1550.
- [28] S. S. Hegedus, W. N. Shafarman, *Prog. Photovoltaics* **2004**, *12*, 155.
- [29] Y. Zhao, S. Yuan, D. Kou, Z. Zhou, X. Wang, H. Xiao, Y. Deng, C. Cui, Q. Chang, S. Wu, *ACS Appl. Mater. Interfaces* **2020**, *12*, 12717.
- [30] J. Chantana, T. Nishimura, Y. Kawano, S. Teraji, T. Watanabe, T. Minemoto, *ACS Appl. Energy Mater.* **2019**, *2*, 7843.
- [31] J. Wong, S. T. Omelchenko, H. A. Atwater, *ACS Energy Lett.* **2020**, *6*, 52.
- [32] a) M. Raghuvanshi, M. Chugh, G. Sozzi, A. Kanevce, T. D. Kühne, H. Mirhosseini, R. Wuerz, O. Cojocar-Mirédin, *Adv. Mater.* **2022**, *34*, 2203954; b) T. Schneider, C. Dethloff, T. Hölscher, H. Kempa, R. Scheer, *Prog. Photovoltaics* **2021**, *30*, 191.
- [33] J.-H. Kim, M. K. Kim, A. Gadisa, S. J. Stuard, M. M. Nahid, S. Kwon, S. Bae, B. Kim, G. S. Park, D. H. Won, D. K. Lee, D.-W. Kim, T. J. Shin, Y. R. Do, J. Kim, W. J. Choi, H. Ade, B. K. Min, *Small* **2020**, *16*, 2003865.